A MICROMIRROR FOR OPTICAL PROJECTION DISPLAYS

R.A.Brookhuis[1], M.J. de Boer[1], M. Dijkstra[1], A.A. Kuijpers[2], D. van Lierop[2] and R.J. Wiegerink[1]

[1]*MESA+ institute for nanotechnology, University of Twente, Enschede, The Netherlands*
[2]*Philips Applied Technologies, Eindhoven, The Netherlands*

***Abstract* — In this paper we present a tilting micro mirror with a large mirror surface of up to 2.5 mm x 1.0 mm and a large rotation angle of +/- 10° as needed for optical projection displays. The mirror is driven by vertical comb-drive actuators which are realized by a combination of deep reactive ion etching (DRIE) and a buried mask to provide self-alignment of the stator and rotor fingers in a silicon on insulator (SOI) wafer. Measurement results are shown for various realized mirror designs.**

Keywords : **micromirror, vertical comb-drive, SVC, DRIE, laser display, pocket projector.**

I - Introduction

Miniature laser projection or pico projection is one of the most promising technologies [1] for displaying information from small electronic devices like mobile phones, PDA's and multi-media players. The current possibilities with micro technology and the availability of tiny light sources which can be modulated at high frequencies give the possibility of making an efficient projection system in a very small form factor. This is of interest for mobile applications or other applications where weight, low power consumption and form factor are important design rules.

The micro mirror presented in this paper is meant for a bidirectional scanning system with a small 'fast' mirror for the horizontal scan direction and a larger 'slow' mirror for the vertical direction. The 'fast' mirror, which operates in resonance, has been presented earlier [2-3]. In this paper we present a tilting micro mirror with a large mirror surface as a solution for the 'slow' mirror. This mirror will not be driven in resonance, but with a 50 Hz saw-tooth signal, which means that the bandwidth should be in the order of 1 kHz to obtain a fast retrace time. In Figure 1 a schematic diagram is shown of a laser based projection display. The projector consists of three light sources and two mirrors which deflect the light beam. One mirror deflects the light over the horizontal axis and the other mirror deflects the light over the vertical axis. Doing so, the light can be steered over a 2D plane. To be able to create a color and differences in brightness, the three light sources are modulated at high frequency to vary the intensity.

An overview of previously published micromirrors can be found in [4-5].

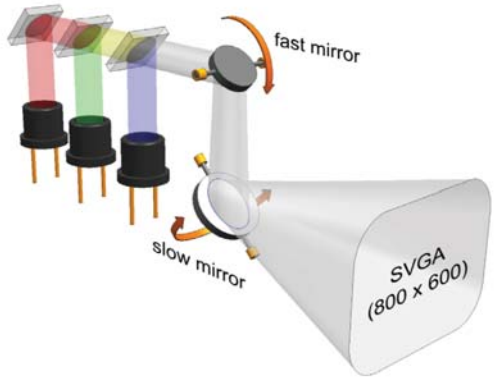

Figure 1: *Model of a laserdiode based projection system consisting of 3 laser diodes (red, green, blue) and two mirrors to deflect the light over two perpendicular axes. Color is created by modulating the light source with an on-off signal to vary its intensity (image taken from [2]).*

II - Design

A. Mirror Design

In Figure 2 the model of the micromirror is shown. The mirror is suspended by two torsion axes with a rectangular cross-section and the actuation is done by a staggered vertical comb-drive (SVC) [6-8]. To create two nicely defined levels, an SOI wafer is used. The mirror surface should have good reflective properties and must ensure that the reflection characteristics are such that the resolution of the whole system is diffraction limited. The static flatness is determined by the residual stress in the mirror surface. The dynamic flatness is determined by the rigidity of the mirror surface and the angular acceleration. Due to the moment of inertia of the mirror, the surface will deform in an s-curve as shown in [9]. The deflection due to angular acceleration together with the initial curvature of the mirror should not exceed $\lambda/10$, which means that the flatness should be below 40 nm. Table 1 summarizes the target specifications for the mirror device.

Table 1: *Target mechanical and electrical properties*

Property	**Symbol**	**Specification**
Mirror width	w_m	1000 µm
Mirror length	l_m	2500 µm
Maximum rotation angle	θ_{max}	-10° to +10° (mechanical)
Maximum actuation voltage	u_{max}	60 Volt
Mirror flatness	δ_{max}	λ/10 (< 40 nm)

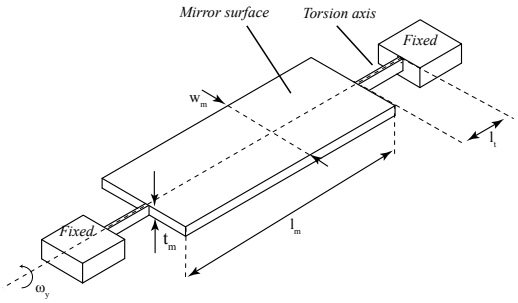

Figure 2: *Model of the 1D micromirror*

B. Comb-drive Actuator

The mirror will not be operated in resonance. This means that the SVC actuator must actuate the mirror surface over the full range. The maximum static rotation angle which can be achieved is determined by the height and length of the comb-fingers. This maximum occurs where the overlapping area between the stator and rotor comb has a maximum. Due to the geometry, the change in area is not fully linear up to the maximum overlap. The angle for which the change in area is assumed to be linear occurs at θ_{mlin} where the upper-right corner of the rotor comb is at the same height as the topside of the stator comb finger, see Figure 3. To express the capacitance as function of the angle of rotation θ, the model will be simplified by defining the rotation axis on the same horizontal plane as the bottom of the stator comb (see Figure 3b). This yield the following expression for the capacitance as function of the angle θ:

$$C_{svc}(\theta) = N_f \frac{\epsilon_0 \epsilon_r \left(l_f^2 - l_{so}^2\right)}{g_{rs}} \theta \qquad (1)$$

Where N_f is the number of fingers, l_f the length of the rotor finger, l_{so} the offset of the stator from the center of rotation and g_{rs} the gap spacing between the rotor and the stator. From this equation the torque exerted by the vertical comb-drive as a function of the applied voltage can be expressed when taking the derivative of the capacitance to θ at constant voltage u while neglecting the fringing field effect:

$$\tau_{el} = N_f \frac{\epsilon_0 \epsilon_r \left(l_f^2 - l_{so}^2\right)}{2 g_{rs}} u^2 \quad if\ 0 \le \theta \le \theta_{\text{mlin}} \qquad (2)$$

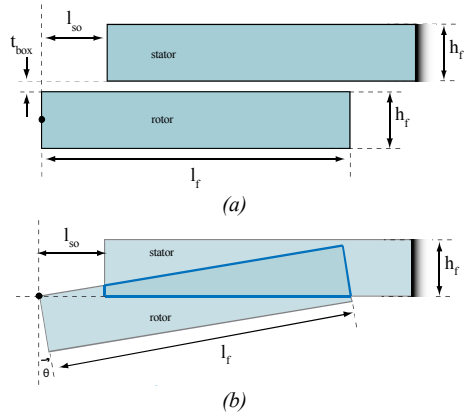

Figure 3: *Schematic view of the vertical comb-drive actuator with (a) initial position (b) model for actuated comb-drive.*

Figure 4 shows the calculated capacitance using FEM simulations. The resulting curve is almost identical to the analytical expression given by (2) for $\theta_{\text{mlin}} = 10°$.

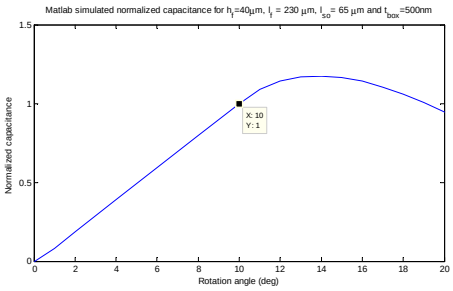

Figure 4: *FEM results showing normalized change in capacitance versus rotation angle for h_f = 40 um, l_f = 230 µm, l_{so} = 65 µm and t_{box} = 500 nm. The capacitance is normalized at θ_{mlin} = 10°.*

C. Position Sensing

For controlling the mirror and the projector, the angle of rotation of the mirror needs to be known. For SVGA resolution the required angular resolution is 0.03 degrees. Commonly used position sensing mechanisms are capacitive sensing, piezo-electric sensing [10-11] and thermal displacement sensing. Capacitive rotation angle measurement is compatible with the fabrication process. If designed well, the parasitic effects of a capacitive measurement can be suppressed by a differential measurement which suppresses all common mode signals. A disadvantage of a capacitive sensing method is that the measurement introduces parasitic forces which can be suppressed by using differential measuring methods with frequencies way above the mechanical bandwidth of the system. To cancel out the actuation signal, two actuator groups are realized on each side of the mirror. One group is actuated by a positive signal, the other group by the same signal with opposite polarity.

III - Fabrication

A. Process flow

Figure 5 shows the outline of the process flow. **(a)** The base material is a SOI wafer with a device layer of 40 µm, a handle layer of 340 µm and a buried oxide layer of 500 nm. **(b)** The handle layer will be etched until there is a thickness equal to $h_f = 40\ \mu m$ left. This etch determines the height of the rotor comb-fingers and the thickness of the mirror surface. **(c)** A 1200 nm TEOS SiO_2 layer is deposited, to form a stopping layer which is needed later (in steps k and l). LPCVD SiO_2 is chosen because this is, after deposition, slightly tensile compared to silicon. A layer of 150 nm Chromium is deposited on the backside. This is to ensure good thermal conductivity which is required to control the wafer temperature during DRIE etching in step k and l. **(d,e)** Patterning of photoresist and etching of SiO_2 in which the stator fingers are defined and all other features which should not be etched during all the steps. In this

step, the width of the stator fingers is 2 µm wider than the final width. This allows a tolerance in the alignment between the lithography steps *i* and *g*. **(f,g)** Second photoresist patterning step and SiO_2 etch in which the rotor fingers and mirror surface are defined. The pattern must be deposited within 2 µm alignment of the previous step. The misalignment is etched away by a second SiO_2 etch. At the places where there is no masking layer, the silicon will be completely etched to the SiO_2 stopping layer. Everywhere where there is only photoresist, the silicon will be etched to the buried oxide (BOX) layer. **(h)** First DRIE [12] step (DRIE-1), which will stop on the BOX layer. The recipe for etching DRIE-1 must have straight sidewall profiles and no notching. **(i)** Removal of the buried oxide layer. As described in [8], etching SiO_2 in high aspect ratio trenches can lead to unexpected results. For this step a custom recipe has been developed which make use of CHF_3 with high ion bombardment. **(j)** Second DRIE step (DRIE-2), which will stop on the SiO_2 stopping layer. When the silicon is etched away, the mirror surface is only connected to the substrate by the torsion axis. Since high energies are involved in the etching process the mirror surface will heat up and eventually the torsion axis will be damaged due to thermal effects. Therefore a layer of chromium is deposited in step c. **(k)** Stripping of photoresist. Last DRIE step (DRIE-3), which will remove the upper part of the rotor comb-fingers. **(p)** Removal of the chromium layer by O_2 plasma. Vapor HF is used to etch the Silicon Dioxide stopping layer, which releases the mirror.

B. Fabrication results

Figure 6 shows a photograph of the scanning micromirror and a close-up of the actuator part.

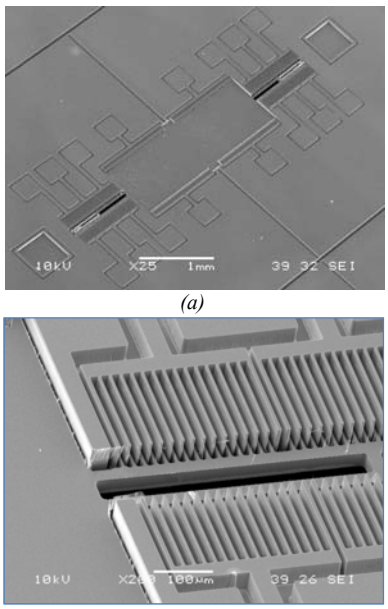

(a)

(b)

Figure 6: *SEM photo showing (a) total overview of the fabriacted micromirror. (b) close-up of the vertical comb-drive actuator.*

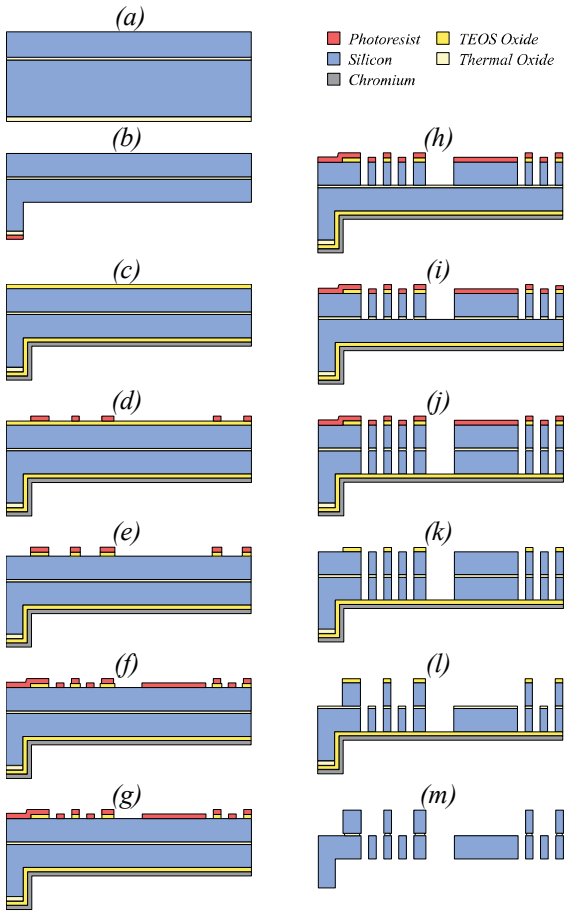

Figure 5: *Process outline (see text).*

IV - Characterization

A. Static behavior

For all samples the static and dynamic properties are determined. Figure 7 shows the measured rotation angle as a function of the actuation voltage for a typical sample with the dimensions shown in table 1. The measured resonance frequency of this device is 243 Hz. It has a finger gap spacing of $g_{rs} = 5\,\mu m$ and the number of comb-fingers used for static actuation (N_f) is 30. In the same figure, the plot of the analytical model with the same bandwidth and gap spacing is shown. As can be seen, the measured values are slightly lower than the analytical values. This is the result of undercut and negative taper of the comb-fingers due to the DRIE process. This increases the gap distance and will therefore result in a lower torque.

B. Dynamic behavior

In Figure 8 the frequency response of various mirror types is shown. Two resonance peaks can be observed the first resonance peak is the desired torsional mode. The second peak in the figure is the out-of-plane sliding mode, where the mirror slides up and down in the direction perpendicular to the mirror surface. Two other higher modes the in-plane sliding and rotational mode

[9] could not be measured with the vibrometer, since these are in-plane motions.

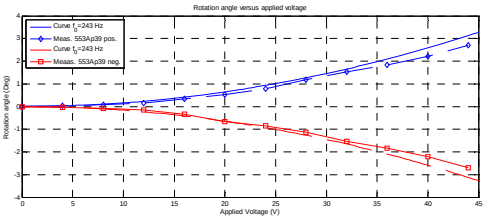

Figure 7: *Rotation angle versus voltage for a sample with resonance frequency of $f_0 = 243$ Hz, and the solid line shows the plot of the analytical model for $f_0 = 243$ Hz, $N_f = 30$ and $g_s = 5$ µm*

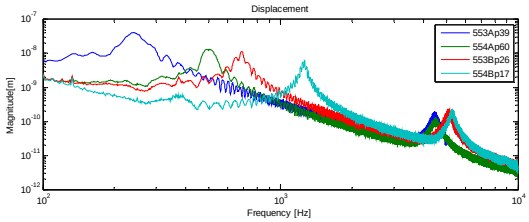

Figure 8: *Polytec MSA 400 vibrometer measurement with a periodic chirp from 1 Hz to 10 kHz for various mirror versions.*
553A: mirror size 2.5x1.0mm, torsion axis width 3 µm.
554A: mirror size 2.5x1.0mm, torsion axis width 4 µm.
553B: mirror size 1.75x0.7mm, torsion axis width 3 µm.
554B: mirror size 1.75x0.7mm, torsion axis width 4 µm.

C. Mirror flatness

Figure 9 (a) shows the three dimensional profile of the silicon mirror surface with 2500 µm length and 1000 µm width. The mirror shows a hollow profile with a maximum deflection δ_m of 30 nm over the length of the mirror and 8 nm over the width of the mirror. Both deflections are below the requirement of 40 nm. In Figure 9 (b) the deflection is plotted against the position on the mirror surface where the center of the mirror surface is the origin. Note that the measurements are performed on a mirror surface without reflective coating.

IV - Conclusions

In this paper we discussed the design, fabrication and characterization of an electrostatically actuated scanning MEMS micromirror for a system based on a two-mirror (2x1D) architecture. The measured resonance frequencies are lower than predicted by the analytical model. This is mainly caused due to tolerances in the pattern transfer (lithography), undercut and sidewall tapering in the DRIE process. Current research focuses on techniques to reduce the mass of the mirror without sacrificing static and dynamic flatness in order to reach a 1 kHz resonance frequency also for the largest mirrors.

Acknowledgements

This work has been sponsored in part by the Dutch government within the Point-One framework MEMS-Land.

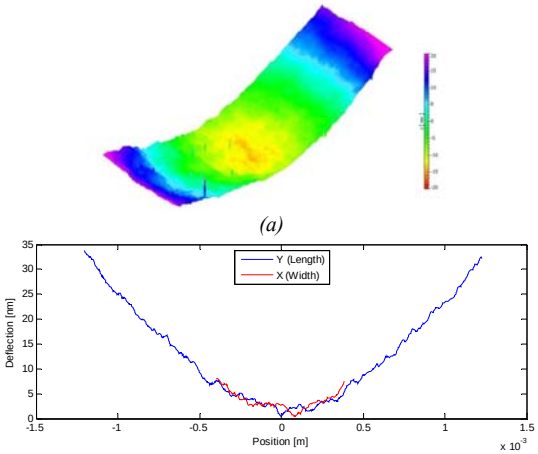

Figure 9: *(a) Three dimensional profile of the silicon mirror surface of 2500x1000 µm without reflective layer measured with the polytech MSA400 white light interferometer. (b) Height profile in x-direction and y-direction of silicon mirror of 2500x1000 µm.*

References

[1] C. Chinnock, "The picoprojector gold rush," *Information Display,* vol. 24, p. 12, 2008.

[2] R. Sanders, *et al.*, "Design and fabrication of a MEMS mirror for miniature laser projection," in *OEMS and Miniaturized Systems VIII*, 2009.

[3] A. Kuijpers, *et al.*, "Towards embedded control for resonant scanning MEMS micromirror," *Procedia Chemistry,* vol. 1, pp. 1307-1310, 2009.

[4] K. Hane and M. Sasaki, "Micro-Mirrors," in *Comprehensive microsystems*, ed: Elsevier B.V. , 2007, p. 2100.

[5] P. Patterson, *et al.*, "Scanning micromirrors: An overview," 2004, p. 195.

[6] R. Conant, *et al.*, "A flat high-frequency scanning micromirror," 2000, pp. 6–9.

[7] K. Kumar and X. Zhang, "CMOS-compatible 2-axis self-aligned vertical comb-driven micromirror for large field-of-view microendoscopes," 2009, p. 1015.

[8] D. Hah, *et al.*, "A self-aligned vertical comb-drive actuator on an SOI wafer for a 2D scanning micromirror," *Journal of Micromechanics and Microengineering,* vol. 14, p. 1148, 2004.

[9] H. Schenk, "Ein neuartiger Mikroaktor zur ein- und zweidimensionalen Ablenkung von Licht," 2000.

[10] M. Sasaki, *et al.*, "Piezoresistive rotation angle sensor integrated in micromirror," *Japanese journal of applied physics,* vol. 45, p. 3789, 2006.

[11] T. Sandner, *et al.*, "Integrated Piezo-resistive Positionssensor for Microscanning Mirrors," 2007, pp. 195-196.

[12] H. Jansen, *et al.*, "Black silicon method X," *Journal of Micromechanics and Microengineering,* vol. 19, 2009.